Elastic scattering of polarized protons from ^{58}Ni at $E_p = 192$, 295, and 400 MeV

H. Sakaguchi,[1] H. Takeda,[1] S. Toyama,[1] M. Itoh,[1] A. Yamagoshi,[1] A. Tamii,[1] M. Yosoi,[1] H. Akimune,[2] I. Daito,[2] T. Inomata,[2] T. Noro,[2] and Y. Hosono[2]

[1]*Department of Physics, Kyoto University, Kyoto 606-01, Japan*

[2]*Research Center for Nuclear Physics, Osaka University, Suita, Osaka 567, Japan*

(Received 25 August 1997)

Elastic scattering of polarized protons from ^{58}Ni has been measured at incident proton energies of 192, 295, and 400 MeV. Optical model calculations employing relativistic impulse approximations and a microscopic folding model using a nonrelativistic G matrix are compared with the experimental results. In order to explain the experiment further, it is necessary to use a density distribution deduced from the charge distribution measured by electron scattering and to modify the nucleon-nucleon interaction in the nuclear medium by altering coupling constants between nucleons and mesons and also adjusting the masses of exchanged mesons. [S0556-2813(98)01804-4]

PACS number(s): 25.40.Cm, 24.10.Jv, 24.70.+s, 27.40.+z

I. INTRODUCTION

Elastic scattering of protons has been successfully employed as a probe to discern various microscopic approaches for nuclear interactions, because the ground state wave function of the target nucleus used for elastic scattering is restricted by the charge distribution measured by electron scattering and thus ambiguities due to the nuclear structure are relatively small. In the 1980s, elastic scattering of polarized protons at medium energies was an issue of long debate between the relativistic and the nonrelativistic approaches. After the success of Dirac phenomenology [1–5] to explain even the polarization observables, we are at a stage to understand the scattering microscopically with the relativistic formalism. At intermediate energies the relativistic impulse approximation (RIA) seems to explain the proton elastic scattering qualitatively by folding the nucleon-nucleon (N-N) interaction with the density distribution of the target nucleus. Murdock and Horowitz [6] have calculated the proton elastic scattering off ^{16}O, ^{40}Ca, and ^{208}Pb between 200 and 400 MeV using the RIA and obtained qualitative agreement with experimental data. Their calculation reproduces the polarization observables remarkably well. Tjon, Wallace, and Ottenstein [7,8] have calculated the elastic scattering off ^{40}Ca by the RIA (IA2) based on the general representation of the N-N scattering amplitudes in the full Dirac space and obtained good agreement with experimentally observed differential cross sections at 800 MeV. Thus the RIA seems to relate the N-N interaction inside the nucleus directly to the nuclear reaction. By using the RIA we are now in a position to investigate a change in the N-N interaction inside the nucleus, namely, a medium effect. On the other hand, the Hamburg group has proposed a nonrelativistic G matrix [9,10] which can be used for the optical potential at intermediate energies. They have calculated the elastic scattering of protons off ^{12}C at 200 MeV and described the experimental results. At present most of the experimental data at intermediate energies are limited to double closed shell nuclei such as ^{40}Ca [11,12], ^{90}Zr [13] and ^{208}Pb [12,13]. It is therefore interesting to measure elastic scattering for other nuclei, to compare their predictability at intermediate energies, where the nonrelativistic potential changes its wein-bottle-bottom shape drastically from attractive to repulsive, and to examine whether we need medium effects to explain the scattering. In this paper, we report data on differential cross sections and analyzing power angular distributions for ^{58}Ni at $E_p = 192$, 295, and 400 MeV in scattering angles between 5° and 45° in the center-of-mass system.

II. EXPERIMENT

The experiment has been performed at RCNP. Polarized protons from an atomic-beam-type ion source were injected to the $K=120$ AVF cyclotron, accelerated to 65 MeV (53 MeV, 39 MeV) for the experiments of final energy 400 MeV (295 MeV, 192 MeV), and transported to the six-sector Ring Cyclotron of $K=400$. Before injecting the beam into the Ring Cyclotron and after extracting it from the Ring Cyclotron, beam polarization was measured continuously by sampling-type beam line polarimeters at intervals of 10–30 sec [14]. Before injection, elastic scattering from the carbon in a CH_2 foil was measured by CsI detectors for the estimation of the beam polarization. After the extraction from the Ring Cyclotron, p-H scattering in a CH_2 foil was utilized for the beam line polarimeter by using coincident scattered proton and recoiled proton signals. Background events from the reaction of ^{12}C $(p,2p)$ were estimated by measuring $(p,2p)$ events from the pure carbon target in a separate run. A typical beam polarization was approximately 65%. After acceleration to the final energy of 400 MeV (295 MeV, 192 MeV), the polarized beam was extracted, passed through the second beam line polarimeter, and transported to the target center. The beam energy from the Ring Cyclotron was calibrated [15] by using two-body kinematics. We measured the angles where peaks from p-H elastic scattering and p-^{12}C inelastic scattering overlapped in the energy spectrum. Using Q values for the reaction, the incident proton energy was calculated, assuming the same magnetic field distribution for various magnetic fields and a linear relation between the momentum and the magnetic field measured by the NMR probe embedded in the spectrograph. The accuracy of the beam energy thus measured was about ± 2 MeV. A typical beam

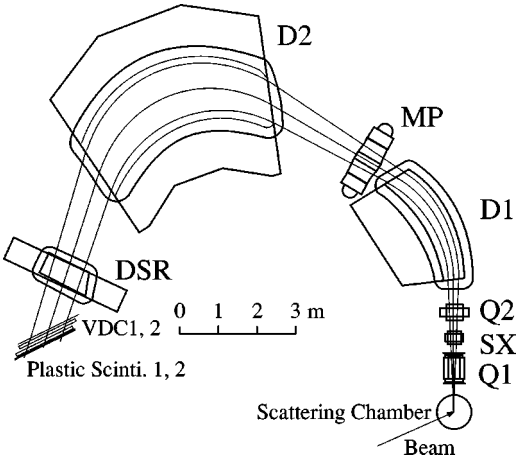

FIG. 1. Schematic view of the high resolution magnetic spectrograph ''Grand Raiden.''

spot size was 1 mm (height) $\times$ 3 mm (width). In order to reduce the background and the beam halo we did not use the slit system in the beam transport line. The beam halo was monitored by plastic scintillators placed along the beam line. Finally, the beam was stopped by an internal Faraday cup made of a 10.5-cm-thick tantalum block placed inside the scattering chamber. The charge collection efficiency of the Faraday cup was calibrated by a large specially made Faraday cup in separate runs and was found to be consistent within a 3% error. The integrated beam current was monitored by a current digitizer. The beam current incident on the target was altered between 0.5 and 5 nA, depending on the scattering angle. The beam current was limited by the dead time of the data-taking system at forward angles and by the leak current of the wire chamber at backward angles. The dead time of the data-taking system was kept less than 10% during the beam time. For the ^{58}Ni target, two kinds of self-supporting metal foils of 5.86 mg/cm^2 (99.9% enrichment) and 100.1 mg/cm^2 (99.9% enrichment) were used for forward angles and backward angles, respectively. Scattered protons were analyzed by a QSQDMD (Q: quadrupole; S: sextupole; D: dipole; M: multipole) type magnetic spectrometer named ''Grand Raiden.'' The maximum magnetic rigidity of the spectrometer was 5.4 Tm, and the momentum dispersion of the spectrograph was 21.35 m. A schematic design of the high resolution magnetic spectrograph Grand Raiden is shown in Fig. 1. Since particles cross the focal plane at an inclination of 45°, the momentum spectrum of the proton was detected by two sets (X, U and X', U') of vertical drift chambers (VDC's) each with an effective area of 120 cm (width) $\times$ 10 cm (height) which were placed in the focal plane of the spectrometer. The maximum drift length of the VDC was 1.0 cm. For reading the VDC signals we used a drift-chamber read-out system supplied by LeCroy. The data collection and monitoring were performed using a VAX work station with the J11 combined with the on-line analyzer of the Q system developed at LAMPF. The start signal for the VDC's was taken from the coincident signals of the two layers of 1-cm-thick plastic scintillators placed down stream of the VDC. Data reduction was performed off line. From the position and angular data obtained from the VDC measurements, we constructed position spectra in the focal plane. Because of the energy spread of the beam, the total energy

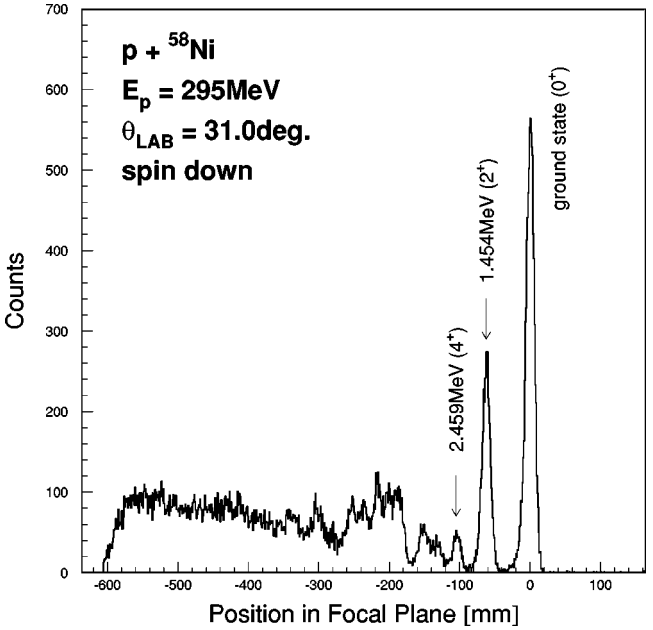

FIG. 2. A typical position spectrum of Grand Raiden for the proton scattering off ^{58}Ni.

resolution of the obtained energy spectrum was about 300 keV. In Fig. 2 we show a typical position spectrum of the proton scattering off ^{58}Ni nuclei. Cross sections and analyzing powers are calculated by correcting for the efficiencies of the wire chambers for each run. In Fig. 3 we display our measured cross sections and analyzing powers.

III. DISCUSSION

In this section we compare our data with the prediction of three types of models, two relativistic impulse approximations and a nonrelativistic microscopic model. Then we attempt to improve the agreement by using realistic densities of the target nuclei and by modifying the coupling constants and the masses of exchanged mesons in the N-N interaction as a medium effect.

A. Model comparison

First we compare our experimental data with the RIA calculations of Murdock and Horowitz [6] (MH). The solid curves in Fig. 3 represent the RIA calculations with the Pauli-blocking effect correction used in the method of MH. The density distributions (vector and scalar densities for protons and neutrons) used for the ^{58}Ni target nuclei were calculated using the relativistic Hartree (RH) approximation of Horowitz and Serot. These are shown in Fig. 4. Although the solid curves in Fig. 3 reproduce the analyzing power precisely, the angular distributions of the cross section are poorly reproduced, especially at backward angles (larger than 30°), where the momentum transfer is more than 2 fm^{-1}. Since cross sections at forward angles, where the Rutherford scattering is the dominant mechanism, are reproduced quite well by the calculation, the ambiguity in the absolute value of the experimental cross section is small. This tendency is the same for all three energies. The dashed curves in the figure represent the calculation [16] employing

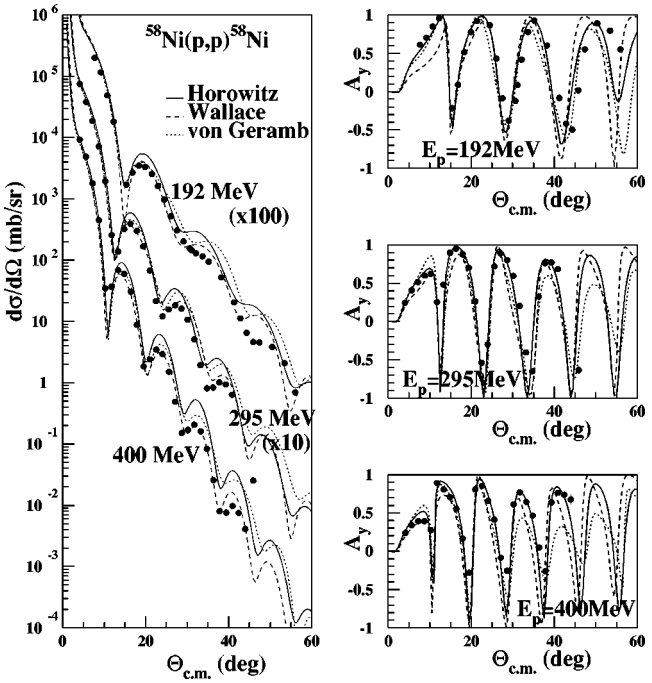

FIG. 3. Experimental data for the elastic scattering off ^{58}Ni at 192, 295, and 400 MeV. The solid curves and the dashed curves correspond to the relativistic impulse approximation calculation using the interaction of the relativistic Love-Franey model of Horowitz and co-workers and the interaction of Tjon and Wallace, respectively. The dotted curves represent the nonrelativistic microscopic optical potential calculations using the *G* matrix of von Geramb. These three models fail to explain the angular distributions of differential cross sections in this energy region.

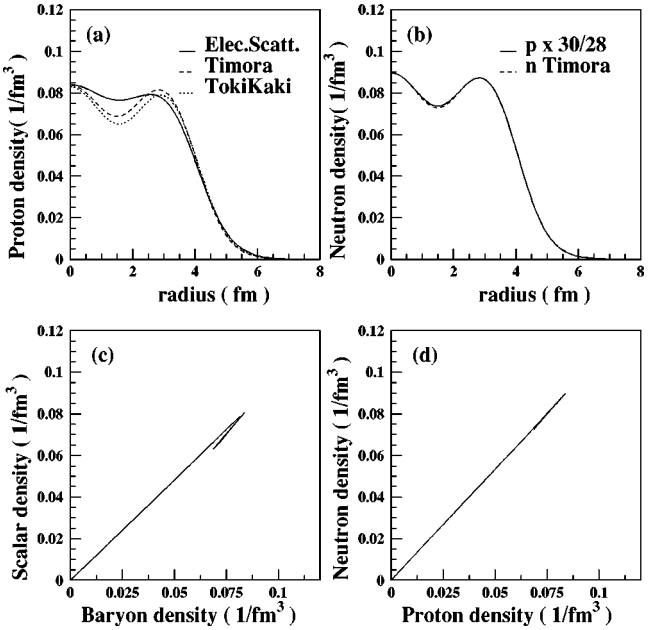

FIG. 4. Various densities used in the RIA calculations. (a) Point proton densities are shown. The solid curve is a density distribution deduced from the charge distribution measured by electron scattering. The dashed curve represents the proton density determined by the relativistic Hartree calculation of Horowitz and Serot. The dotted curve represents a relativistic Hartree calculation performed by Kaki with different parameters and the nonlinear meson field of Toki. (b) Relative shapes for the point proton and the point neutron distribution are compared. The solid curve is the calculated point proton distribution multiplied by 30/28, which is equal to the neutron distribution, assuming the proton and neutron distributions are the same. The dotted curve is the neutron distribution calculated using the relativistic Hartree code. (c) The baryon density for protons and the scalar density for protons are compared for the ^{58}Ni nucleus. (d) The baryon densities for protons and neutrons are compared for the ^{58}Ni nucleus.

the RIA IA2 by Tjon and Wallace [7]. The density distribution was calculated with the RH approximation using the parameter TM2 [17] of Toki, which is capable of reproducing even the density distribution of unstable nuclei [18]. The TM2 parameter gives almost the same baryon density as the calculation of Horowitz and Serot as indicated by the dotted curve in Fig. 4(a). The IA2 calculation reproduces the experimental results at 400 MeV, except at backward angles. At 192 MeV and 295 MeV it overestimates the cross section, as shown in Fig. 3. The predicted analyzing powers deviate from those observed experimentally at 192 MeV. The IA2 model seems to predict the cross sections better than the approach of MH at all three energies. However, with regard to the analyzing power the IA2 prediction is worse than that of MH. The dotted curves in Fig. 3 represent the calculation of the scattering using a nonrelativistic Schrödinger-type optical potential. We have calculated the nonrelativistic Schrödinger optical potential using the *G* matrix of von Geramb [9], following the procedure of Rikus and von Geramb [10]. The density distribution used was obtained by unfolding the free proton charge form factor from the charge distribution of the sum of Gaussian type [19] deduced from electron scattering experiments. At 192 MeV the nonrelativistic optical potential explains the experiments fairly well, providing a description nearly equivalent to that provided by the RIA approaches. It also overestimates the cross section at backward angles. For Ay the prediction deviates from the experiments even at 192 MeV. In general, as the incident energy increases, the deviation between the prediction given by the method of von Geramb and the experimental values increases. In particular, this deviation is large in analyzing powers at 400 MeV. In summary, none of the three models listed above can satisfactorily explain the experimental data. This is true in particular with regard to differential cross section data. Among the three models, only that of MH explains the analyzing power precisely.

B. Ratio of the coupling constants

Before setting out on a search for the medium effect, we consider the sensitivity of polarization observables on meson-nucleon coupling constants. As is shown in Fig. 5, if we increase the coupling constants of the sigma and omega mesons by 10%, for example, holding their relative ratio constant, the analyzing power and the *Q* parameter change very little, while the cross section increases according to the increase of the coupling constant as indicated by the dashed curves. The solid curves represent the original calculations of MH. In these calculations we have used the original density distributions generated by the RH calculation. Even if we increase both of the coupling constants by 50%, the deviation of the angular distribution of polarization observables is quite small as shown in Fig. 6, and the original form of the

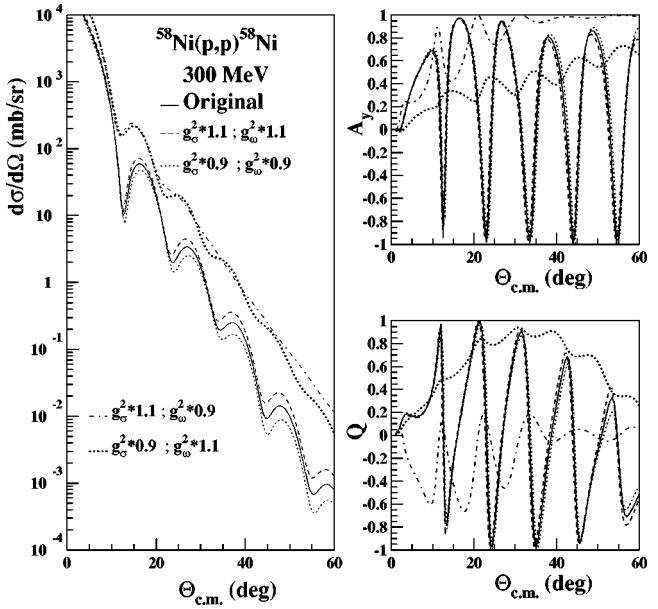

FIG. 5. RIA calculations with different meson-nucleon coupling constants. Solid curves correspond to the original RIA calculation of the Horowitz type. The dashed curves represent the calculations with coupling constants increased by 10% for both the sigma meson-nucleon case and the omega meson-nucleon case, while the dotted curves display the calculation with coupling constants decreased by 10% for both of them. The dot-dashed curves represent the calculation with a 10% increase of the sigma meson-nucleon coupling constant and a 10% decrease of the omega meson-nucleon coupling constant. The thick-dotted curves correspond to calculations with a 10% decrease of the sigma meson-nucleon coupling constant and a 10% increase of the omega meson-nucleon coupling constant. If we maintain the ratio between sigma and omega mesons, polarization observables are stable.

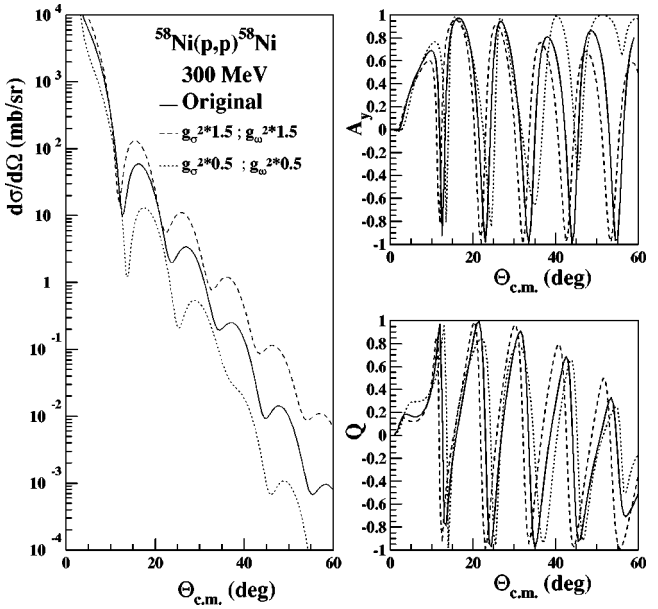

FIG. 6. RIA calculations with different meson-nucleon coupling constants. Solid curves represent the original RIA calculation of the Horowitz type. The dashed and the dotted curves correspond to the calculations with a 50% increase of coupling constants (i.e., $f_\sigma^2 \rightarrow 1.5 f_\sigma^2$ and $f_\omega^2 \rightarrow 1.5 f_\omega^2$) and a 50% decrease of coupling constants (i.e., $f_\sigma^2 \rightarrow 0.5 f_\sigma^2$ and $f_\omega^2 \rightarrow 0.5 f_\omega^2$) for both sigma meson-nucleon and omega meson-nucleon constants, respectively.

angular distribution is maintained. But if we decrease one of the coupling constants by 10% while increasing the other coupling constant by 10% (i.e., $f_\sigma^2 \rightarrow 0.9 f_\sigma^2$ and $f_\omega^2 \rightarrow 1.1 f_\omega^2$), we obtain quite different angular distributions of the polarization observables as shown by the thick dotted curves in Fig. 5. If we reverse the changes in coupling constants ($f_\sigma^2 \rightarrow 1.1 f_\sigma^2$ and $f_\omega^2 \rightarrow 0.9 f_\omega^2$), the situation is similar as depicted by the dot-dashed curves in the figure. Thus we understand that the reason the model of MH is able to describe the behavior of polarization observables is that the ratio of the coupling constants of the sigma meson-nucleon and the omega meson-nucleon used in this model is near the true value. Although ten mesons are used in the MH model for the N-N interaction, coupling constants other than those of sigma and omega mesons affect the predictions only slightly.

C. Distribution of baryon and scalar densities in ^{58}Ni

In order to focus on the problem of the medium effect, we adopt the density distribution obtained by unfolding the free proton charge form factor from the charge distribution of the sum of Gaussian type deduced from the electron scattering experiment [19]. However, for the RIA we need four types of density distributions, namely, baryon and scalar densities of protons and neutrons. According to the calculation of RH [20], using the computer code by Horowitz *et al.* [21], the ratio of the scalar density to the baryon density for the ^{58}Ni nucleus is almost constant and equal to 0.96, as is shown in Fig. 4(c). In Figs. 4(b) and 4(d) we compare vector densities for neutrons and protons in the same RH calculation code. The ratio of these quantities is also almost constant and equal to 30/28. Thus by partially using the results of the RH calculation we can obtain four types density distributions necessary for the RIA calculation from the electron scattering experiments. In Fig. 7 we show the calculation of the differential cross sections and the analyzing powers for the three proton incident energies. The dashed curves represent the original RIA calculation of MH. The dotted curves represent the calculation using the density distribution deduced from the charge distribution. The dotted curve explains the experiments better, while keeping the quality of the fitting for the analyzing power the same as the original. In the calculations corresponding to the dotted and dashed curves in Fig. 7 we have included the effect of Pauli blocking according to the procedure by Murdock and Horowitz [6]. However, there still exist large discrepancies between the experimentally observed and the predicted cross sections.

D. Search for coupling constants and meson masses

If we continue to use the free N-N interaction inside the nucleus, we cannot account for the cross section at backward angles even by using the most realistic baryon and scalar densities for ^{58}Ni. Thus we need to modify the coupling constants and the masses of exchanged mesons, since their character can be changed in the nuclear medium. In the RIA of the MH model, we use a N-N scattering amplitude of the relativistic Love-Franey model of the following form:

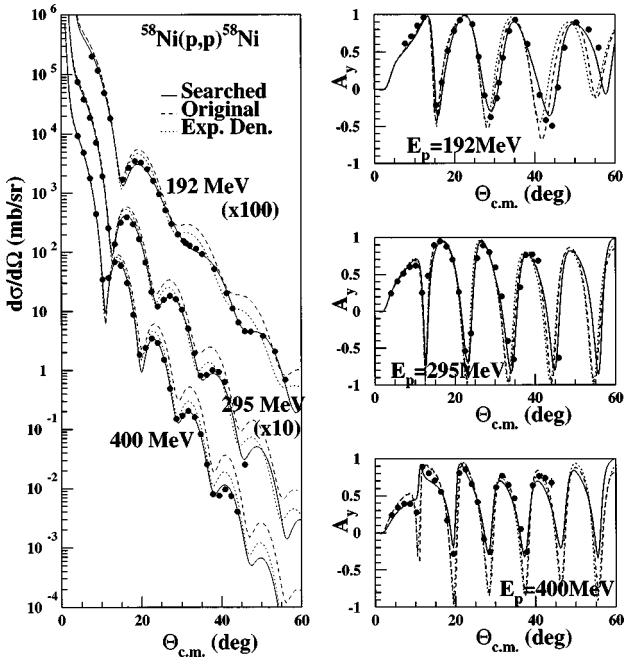

FIG. 7. Experimental data and the RIA calculations with modified interaction. Dashed curves are the results of the original RIA calculation using the code of Horowitz and coworkers and the parameters of the relativistic Love-Franey model. The dotted curves represent a similar calculation as above but using a density distribution deduced from the electron scattering. The solid lines represent a calculation with modified coupling constants and meson masses in the N-N interaction.

$$F=F^S+F^V\gamma^\mu_{(0)}\gamma_{(1)\mu}+F^{PS}\gamma^5_{(0)}\gamma^5_{(1)}+F^T\sigma^{\mu\nu}_{(0)}\sigma_{(1)\mu\nu}+F^A\gamma^5_{(0)}\gamma^\mu_{(0)}\gamma^5_{(1)}\gamma_{(1)\mu}.$$

Here the subscripts (0) and (1) refer to the incident and struck nucleons, respectively. The superscripts S, V, PS, T and A designate scalar, vector, pseudoscalar, tensor, and axial vector parts of the N-N scattering amplitude. The Lorentz invariants F^L ($L=S$, V, PS, T, and A) may be written in the MH model as

$$F^L(q,E_c)=i\frac{M^2}{2E_ck_c}[F^L_D(q)+F^L_X(Q)],$$

$$F^L_D(q)=\sum_j \delta_{L,L(j)}(\tau_0\cdot\tau_1)^{I_j}f^j(q),$$

$$F^L_X(Q)=(-1)^T\sum_j B_{L(j),L}(\tau_0\cdot\tau_1)^{I_j}f^j(Q),$$

$$f^j(q)=\frac{g_j^2}{q^2+m_j^2}\left(\frac{\Lambda_j^2}{\Lambda_j^2+q^2}\right)^2-i\frac{\bar{g}_j^2}{q^2+\bar{m}_j^2}\left(\frac{\bar{\Lambda}_j^2}{\bar{\Lambda}_j^2+q^2}\right)^2,$$

where D and X indicate the direct and exchange terms. The direct and exchange momentum transfers are q and Q, respectively. The coupling constant and mass of the ith meson are denoted by g_i and m_i. The quantities Λ_i and T are the cutoff parameter for the contribution of the ith meson and the total isospin of the two-nucleon system, as defined in Ref. [6], and $B_{L(j),L}$ is the $(L(j),L)$ component of the Fierz transformation matrix [21]. In order to improve the fit to the experimental data, we have changed the coupling constants and masses of the sigma and omega mesons in the above N-N scattering amplitude according to the following formula:

$$g_j^2,\ \bar{g}_j^2\rightarrow\frac{g_j^2}{1+a_j[\rho(r)/\rho_0]},\quad\frac{\bar{g}_j^2}{1+\bar{a}_j[\rho(r)/\rho_0]}$$

$$m_j,\ \bar{m}_j\rightarrow m_j\left[1+b_j\left(\frac{\rho(r)}{\rho_0}\right)\right],\quad\bar{m}_j\left[1+\bar{b}_j\left(\frac{\rho(r)}{\rho_0}\right)\right],$$

$$j=\sigma,\omega.$$

From the survey in the previous subsection, we know that in order to reduce the cross section while maintaining a good reproduction of the polarization observables we must modify the coupling constants while keeping their ratios constant. At each incident energy we have searched for appropriate density-dependent parameters $a_j,\bar{a}_j,b_j,\bar{b}_j$ of the meson-nucleon coupling constants and the meson masses. In free space, where the density of the target is zero, the coupling constants and masses of mesons are arranged to be the same as those of the free N-N interaction, but inside the nucleus the modification is assumed to be proportional to the nucleon density in the above parametrization. If we express various nuclear many-body effects in terms of the nuclear density, which is assumed to be small at a normal nucleus, we can obtain a lowest order approximation of the influence of this density by retaining effects, which are first order in this parameter. The dashed curves in Fig. 7 represent the original Horowitz model calculation. But if we change the four densities to realistic values, as described in the previous section,

TABLE I. Medium effect coefficients for the meson-nucleon coupling constants and the masses of the exchanged meson are shown at each incident proton energy. a_σ ($\bar{a}_\sigma$) is a density-dependent coefficient for the coupling constant of the sigma meson in the real (imaginary) part of the scattering amplitudes. b_σ($\bar{b}_\sigma$) is a density-dependent coefficient of the exchanged sigma meson mass in the real (imaginary) part of the scattering amplitudes.

	g^2_σ		m_σ		g^2_ω		m_ω	
Energy	a_σ	$\bar{a}_\sigma$	b_σ	$\bar{b}_\sigma$	a_ω	$\bar{a}_\omega$	b_ω	$\bar{b}_\omega$
192 MeV	0.1980	0.5948	0.0116	0.1940	0.3415	0.9253	−0.0154	−0.0127
295 MeV	0.1943	0.2506	−0.0009	0.0766	0.2373	0.3448	0.0100	−0.0219
400 MeV	0.3215	0.5294	0.0221	0.2154	0.3506	0.5589	−0.0060	−0.0027

the calculation yields results shown by the dotted curves. In addition, if we introduce the medium modification to the N-N interaction, the calculation gives the solid curves, keeping the fit to polarization observables almost the same. The parameters used here are shown in Table I. Coupling constants decrease about 20–30 %, but the change of the meson masses is at most 2% at normal density. The parameters obtained have a slight spread. They also depend on the initial parameters used in the original relativistic Love Franey interaction. The main part of the decrease of the coupling constants may be in Pauli blocking. Pauli blocking reduces scattering inside the nucleus. If there were no Coulomb potential, the effect of the decrease and the increase of the coupling constants would affect the cross section directly by decreasing and increasing the cross section in the entire angular region. But for the scattering of protons from ^{58}Ni, the scattering amplitudes at forward angles are dominated by the Coulomb part. In the figure, the experimentally determined cross section of forward angles is described well by the calculation. This implies that ambiguities in the absolute values of the experimental cross section are small. Thus the cross section at backward angles reflects scattering by the nuclear interaction, and the original calculation using the MH model overestimates the scattering at backward angles. That is, it overestimates the scattering inside the nucleus. Thus the decrease of the coupling constants may be explained by the Pauli-blocking effect. On the other hand, the decrease in the mass of exchanged mesons may affect the scattering by shifting the diffraction pattern backwards. In our parametrization of the medium effects, the cutoff parameter Λ_i has been kept constant according to the following reasons. The change of the cutoff parameter Λ_i affects the angular distributions only slightly, compared to the large effects caused by the change of the coupling constants and the masses of mesons. The effect of the density dependence of the cutoff parameters is similar to that of the density dependence of the masses of mesons and has been already taken into account effectively by the density dependence of the masses of mesons.

Thus we can fit the experimentally determined angular distribution of the elastic scattering of protons at medium energies by changing the coupling constants and the masses of exchanged mesons. Although many other mesons contribute to the real N-N interaction, it is well known that contributions from mesons other than sigma and omega mesons are negligible to the elastic scattering from $N \cong Z$ nuclei. In other words we can define the medium effect on sigma and omega mesons precisely by studying elastic scattering from $N \cong Z$ nuclei.

According to the theory of Kohmura and co-workers [22], the medium effect of the propagator of exchanged mesons is considered to be the change of the mass operator of the meson propagator:

$$\frac{g_j^2}{q^2+m_j^2} \rightarrow \frac{g_j^2}{q^2+m_j^2+\Pi_j}.$$

Here the additional term Π_j in the above meson propagator is introduced as a medium effect. If we expand Π_j in terms of ρ and q^2, we have

$$\Pi_j = a_j\left(\frac{\rho}{\rho_0}\right) + b_j\left(\frac{\rho}{\rho_0}\right)q^2 + \cdots,$$

$$\frac{g_j^2}{q^2+m_j^2+\Pi_j} = \frac{g_j^2}{q^2+m_j^2+a_j(\rho/\rho_0)+b_j(\rho/\rho_0)q^2}$$

$$= \frac{g_j^2}{[1+b_j[\rho/\rho_0)]q^2+m_j^2+a_j(\rho/\rho_0)}$$

$$= \left(\frac{g_j^2}{1+b_j(\rho/\rho_0)}\right)\left(\frac{1}{q^2+\dfrac{m_j^2+a_j\left(\rho/\rho_0\right)}{1+b_j(\rho/\rho_0)}}\right)$$

$$\approx \left(\frac{g_j^2}{1+b_j(\rho/\rho_0)}\right)\left(\frac{1}{q^2+m_j^2+(a_j-b_j)(\rho/\rho_0)}\right).$$

The above final formula due to Kohmura is similar to our formula of medium modification. Thus by fitting to our experimental data, we are in a position to obtain information on the density and momentum dependence of the additional term of the meson propagator. Here, the reduction of the scattering caused by Pauli blocking is described by the mass operator proportional to the density multiplied by the square of the momentum (ρq^2). On the other hand, the density dependence of the meson mass arises from the difference between the coefficients of the density-dependent term and the term of ρq^2. The origin of the additional term Π_j may be due to the Pauli-blocking effect, the N-N polarization effect on the meson exchange interaction [22], and/or a quark effect [23].

Our results differ from the analysis by Brown *et al.* [24] for the proton elastic scattering off ^{40}Ca, ^{58}Ni, and ^{208}Pb at 500 MeV and 800 MeV. They succeeded in explaining the cross section data by a 15% decrease of the nucleon mass at normal density ρ_0 in the nonrelativistic impulse approximation, which corresponds to a 15% decrease of sigma and omega meson masses. Although they did not give the calculation for polarization observables, their standpoint is the same as ours: By using realistic density distributions and the framework of the impulse approximation, one may derive the medium effect. Since we cannot neglect the Pauli-blocking effect at our incident proton energy between 200 MeV and 400 MeV, we must take this effect into account by introducing a density-dependent coupling constant. In addition, we have introduced different density-dependent coefficients for the real and imaginary parts of the scattering amplitudes. Thus, as is shown in Table I, the obtained parameters have a slight spread. Although ambiguities in the obtained parameters due to error propagation are small (about 10%), there can be some discrete ambiguities in the parameter sets. In order to fix the parameters and to firmly establish the medium effect, we need further systematic experimental data and a theoretical guide for reducing the number of density-dependent parameters.

IV. SUMMARY

We have measured elastic scattering of polarized protons off ^{58}Ni at 192 MeV, 295 MeV, and 400 MeV. The analysis

of the data was performed using two types of relativistic impulse approximations, namely, those of Horowitz, Serot, and Murdock, and Tjon and Wallace. A nonrelativistic microscopic optical potential analysis was also performed by using the G matrix of von Geramb and co-workers. We have found that none of the three models can satisfactorily explain the experimental data. In the relativistic impulse approximation, polarization observables are found to be very sensitive to the ratio of the coupling constants between the sigma mesons and omega mesons to nucleons. By using experimental densities deduced from electron scattering and by modifying the coupling constants and the masses of exchanged mesons in the nucleon-nucleon interaction, we could explain our experimental data at backward angles in the framework of the relativistic impulse approximation. This modification of the nucleon-nucleon interaction in the nuclear medium is attributed to the medium effect. Further systematic studies both from the experimental and theoretical sides are necessary to firmly establish the medium effect.

ACKNOWLEDGMENTS

We would like to thank Prof. Hatanaka and the staff members of the RCNP for their support during the experiment. We wish to acknowledge Prof. H. Toki, Dr. K. Kaki, Prof. T. Kohmura, and Prof. M. Nakano for helpful discussions. We also thank Prof. M. Fujiwara for help during the early stages of the experiment. This experiment was performed at the Research Center for Nuclear Physics under program No. E7 and was supported in part by a Grant-in-Aid for Scientific Research, No. 07640393, of the Japan Ministry of Education, Science, and Culture.

[1] L. G. Arnold, B. C. Clark, R. L. Mercer, and P. Schwandt, Phys. Rev. Lett. **23**, 1949 (1981).
[2] L. G. Arnold, B. C. Clark, and R. L. Mercer, Phys. Rev. C **27**, 2123 (1983).
[3] S. Hama, B. C. Clark, E. D. Cooper, H. S. Sherif, and R. L Mercer, Phys. Rev. C **41**, 2737 (1990).
[4] E. D. Cooper, S. Hama, B. C. Clark, and R. L. Mercer, Phys. Rev. C **47**, 297 (1993).
[5] B. C. Clark, R. L. Mercer, and P. Schwandt, Phys. Lett. **122B**, 211 (1983).
[6] D. P. Murdock and C. J. Horowitz, Phys. Rev. C **35**, 1442 (1987).
[7] J. A. Tjon and S. J. Wallace, Phys. Rev. C **32**, 1667 (1985); **36**, 1085 (1987).
[8] N. Ottenstein, S. J. Wallace, and J. A. Tjon, Phys. Rev. C **38**, 2272 (1988).
[9] H. V. von Geramb, in *The Interaction Between Medium Energy Nucleons in Nuclei*, edited by H. O. Mayer, AIP Conf. Proc. No. 97 (AIP, New York, 1982), p. 44.
[10] L. Rikus, K. Nakano, and H. V. von Geramb, Nucl. Phys. **A414**, 413 (1984); L. Rikus and H. V. von Geramb, *ibid.* **A426**, 496 (1984).
[11] H. O. Meyer, P. Schwandt, R. Abegg, C. A. Miller, K. P. Jackson, S. Yen, G. Gaillard, M. Hugi, R. Helmer, D. Frekers, and A. Saxena, Phys. Rev. C **37**, 544 (1988).
[12] D. A. Hutcheon, Nucl. Phys. **A483**, 429 (1988).
[13] L. Lee, T. E. Drake, S. S. M. Wong, D. Frekers, R. E. Azuma, L. Buchermann, A. Galindo-Uribarri, J. D. King, R. Schubank, R. Abegg, R. Helmer, K. P. Jackson, C. A. Miller, and S. Yen, Phys. Lett. B **205**, 219 (1988); Lee *et al.*, Nucl. Phys. **A492**, 607 (1989).
[14] T. Ichihara, H. Sakaguchi, K. Hatanaka, M. Fujiwara, and K. Hosono, RCNP Annual Report, 1981 (unpublished), p. 194.
[15] T. Noro, K. Hatanaka, K. Hosono, H. Akimune, H. Sakaguchi, M. Yosoi, A. Tamii, and S. Toyama, RCNP Annual Report, 1994 (unpublished), p. 167.
[16] K. Kaki, Nucl. Phys. **A531**, 478 (1991); (private communication).
[17] H. Toki, TMU/RIKEN Summer Institute on Unstable Nuclei Report No. RIKEN-AF-NP-173, p. 37.
[18] D. Hirata, H. Toki, T. Watabe, I. Tanihata, and B. V. Carlson, Phys. Rev. C **44**, 1467 (1991); I. Tanihata, D. Hirata, T. Kobayashi, S. Shimoura, K. Sugimoto, and H. Toki, Phys. Lett. B **289**, 261 (1992); D. Hirata, H. Toki, I. Tanihata, and P. Ring, *ibid.* **314**, 168 (1993).
[19] J. R. Ficence *et al.*, Phys. Lett. **42B**, 213 (1972); I. Sick, *ibid.* **116B**, 212 (1982).
[20] C. J. Horowitz and Brian D. Serot, Nucl. Phys. **A368**, 503 (1981); C. J. Horowitz, Phys. Rev. C **31**, 1340 (1985); C. J. Horowitz and Brian D. Serot, Phys. Lett. B **368**, 220 (1988).
[21] C. J. Horowitz, D. P. Murdock, and Brian D. Serot, *Computational Nuclear Physics 1* (Springer-Verlag, Berlin, 1991), Chap. 7.
[22] S. Kinpara and T. Kohmura, Prog. Theor. Phys. **93**, 659 (1995); A. Kato, S. Kinpara, and T. Kohmura, *ibid.* **94**, 657 (1995); S. Kinpara and T. Kohmura, Nucl. Phys. **A601**, 333 (1996); T. Kohmura, in Proceedings of the RCNP International Mini-workshop on Nuclear Medium Effect via Nucleon Induced Reaction, [Genshikaku Kenkyu **42**, 173 (1997)].
[23] K. Saito, K. Tsushima, and A. W. Thomas, Nucl. Phys. **A609**, 339 (1996); Aust. J. Phys. **50**, 115 (1997); P. A. M. Guichon, K. Saito, E. Rodionov, and A. W. Thomas, Nucl. Phys. **A601**, 349 (1996).
[24] G. E. Brown, A. Sethi, and N. M. Hintz, Phys. Rev. C **44**, 2653 (1991).